RSC Advances

ROYAL SOCIETY OF CHEMISTRY

www.rsc.org/advances

Journal Name

ARTICLE

2,2'-Bis(trifluoromethyl)biphenyl as a Building Block for Highly Ambient-Stable, Amorphous Organic Field-Effect Transistors with Balanced Ambipolarity

Received 00th January 20xx,
Accepted 00th January 20xx

DOI: 10.1039/x0xx00000x

www.rsc.org/

Chi-Jui Chaing,[a] Jyh-Chien Chen,*[a] Yu-Ju Kuo,[a] Hsiang-Yen Tsao,[a] Kuan-Yi Wu,[b] Chien-Lung Wang[b]

Novel conjugated polymers, PBPV-TPA, PBPV-CBZ, PBPV-MEH and PBPV-FLO, consisting of trifluoromethyl-substituted biphenyl (2,2'-bis(trifluoromethyl)biphenyl, CF_3-BP) as the acceptor with various aromatic donors (triphenylamine TPA, carbazole CBZ, 2-(2-ethylhexyloxy)-5-methoxybenzene MEH and fluorene FLO, respectively) have been successfully synthesized. Their amorphous features, confirmed by wide-angle x-ray scattering, small-angle x-ray scattering and atomic force microscopy, are attributed to lateral side chains on the CBZ, MEH and FLO units, and the propeller geometry of the TPA unit. By integration of CF_3-BPs into the polymer backbone, the ambipolarities and well-balanced charge mobilities of OFETs based on these polymers were successfully demonstrated. OFET based on PBPV-FLO exhibits the highest hole mobility of 0.0152 $cm^2 V^{-1} s^{-1}$ and electron mobility of 0.0120 $cm^2 V^{-1} s^{-1}$. In addition, these OFETs also exhibit annealing-free characteristics and ambient stability. The OFET performance without encapsulation remained nearly unchanged in ambient conditions up to 90 days. This could be attributed to the enhanced oxidative stability from their relatively deep HOMO energy levels and better moistures resistance from the trifluoromethyl substitution. Considering the ambipolar, annealing-free and ambient-stable properties of these CF_3-BP-based amorphous conjugated polymers, the electron-accepting CF_3-BP unit can be considered as a promising building block in preparing the easily processable conjugated polymers used in high-stability optoelectronic applications.

Introduction

Conjugated semiconducting polymers have been regarded as one of the key materials to realize organic electronics[1-4] due to their advantageous molecular tailorability,[5-6] tunable optoelectronic properties,[7-8] solution processability[9-10] and compatibility with plastic substrates.[11-12] High charge mobility (μ) is essential to achieve high device performances. OFET based on poly(3-hexylthiophene) (P3HT), which delivered the highest hole mobility of 0.1 $cm^2 V^{-1} s^{-1}$, was once regarded as the benchmark before 1996.[13] The record of charge mobilities based on conjugated polymers has been refreshed over the last two decades. Unprecedentedly high mobility of 47 $cm^2 V^{-1} s^{-1}$ has been demonstrated by capillary-assisted self-assembly on the nanogooved substrates by Heeger.[14] Conjugated polymers with high ambipolar mobilities both exceed 1 $cm^2 V^{-1} s^{-1}$ have also been synthesized by various groups.[9, 15-16] Crystallinity and molecular orientation have been proven important for the organic field-effect transistors (OFETs).[17-19] Molecular aligning processes, such as mechanical rubbing,[20] solvent-vapor[21] and thermal annealing[22-23] have been widely exploited to induce better crystallinity and orientation of the thin-films of conjugated molecules. Although localized crystalline domains in thin films have been demonstrated, extension of these domains across sizable areas and a large number of different discrete devices remains problematic. Moreover, most of these processes are sometimes time-consuming and hard to be modified for roll-to-roll production with reliable reproducibility.

In addition to the morphology and molecular orientation, suitable combination of donor (D) and acceptor (A) conjugated units plays an important role to achieve the ambipolar charge transport characteristics. The ambipolarity of conjugated polymers are generally obtained after efficient acceptors, such as diketopyrrolopyrroles,[24-25] isoindigos,[26] naphthalene diimides,[27-28] and halogens,[29] were incorporated. The incorporation of some acceptors also eased the unacceptable long-term ambient stability of conjugated polymer in the presence of oxygen and moisture by deepening the highest occupied molecular orbital (HOMO) energy levels.[30] Among the electron-accepting moieties, fluorine atoms have drawn extensive attention.[31-32] Due to the strong electronegativity of fluorine atoms, fluorination of conjugated polymers lowers not

[a] Department of Materials Science and Engineering, National Taiwan University of Science and Technology, 43, Sec. 4 Keelung Road, Taipei 10607, Taiwan.
[b] Department of Applied Chemistry, National Chiao Tung University, 1001 Ta Hsueh Road, Hsin-Chu 30010, Taiwan.

Electronic Supplementary Information (ESI) available: [monomer synthesis, solubility, thermal properties, DFT-optimized molecular geometries, AFM, WAXS ring patterns, SAXS ring patterns and additional figures]. See DOI: 10.1039/x0xx00000x

only the lowest unoccupied molecular orbital (LUMO) but also the HOMO energy levels, which facilitates the electron injection from electrodes[33-34] and promotes the oxidative stability,[4] respectively.

In our previous research, 2,2'-bis(trifluoromethyl)biphenyl (CF_3-BP) was integrated into the backbone to construct a novel thienylene-containing conjugated polymer CF_3-PBTV. The n-type characteristic together with balanced ambipolarity and a high on/off ratio was successfully introduced into the p-type thienylenevinylene matrix. High ambient stability without discernable degradation in charge mobility, threshold voltage and on/off ratio was also detected.[35] The ambient stability was attributed to the enhanced oxidative stability from its deep HOMO energy level and better moisture resistance from its hydrophobic trifluoromethyl substitution. Moreover, the favorable annealing-independent OFET performance was found due to its amorphous-like morphology introduced by the non-coplanarity of CF_3-BPs.

In comparison to electron-accepting units, electron-donating building blocks have also been extensively developed recently. The recent emergence of heterocyclic and ladder-type electron donors, including naphthobisthiadiazole,[36] benzodi(cyclopentadithiophene)[37] and indacenodiselenophene,[38] leads to the impressive progress in OFET performances. Compared with these lately-developed electron-donating units, electron donors such as triphenylamine (TPA), carbazole (CBZ), 2-(2-ethylhexyloxy)-5-methoxybenzene (MEH), fluorene (FLO) and their derivatives can be easily prepared and the synthetic procedures are well-established. These units have been comprehensively investigated and utilized in organic light-emitting diodes (OLEDs) in the early stages of conjugated polymer development. However, reports on the OFET performance and ambient stability of conjugated polymers based on these building blocks have been scarce, compared to those on heterocyclic and fused ones. Moreover, OFETs based on TPA, CBZ, MEH and FLO were generally p-type even when strong electron-accepting units, such as thienoisoindigos, benzothiadiazoles and diketopyrrolopyrroles, were incorporated.[39-44]

In this study, we report the synthesis and characterization of four novel solution-processable conjugated polymers (PBPV-TPA, PBPV-CBZ, PBPV-MEH and PBPV-FLO, as shown in Scheme 1) with CF_3-BP as the electron-accepting unit. The ambipolarity and amorphous characteristics are successfully introduced to the p-type TPA, CBZ, MEH and FLO matrix. The annealing-temperature-independent amorphous features are examined carefully by wide-angle x-ray scattering (WAXS), small angle x-ray scattering (SAXS) and atomic force microscopy (AFM). OFETs based on these four polymers are fabricated and characterized in ambient conditions. All OFETs show excellent stability in ambient conditions up to 90 days. Considering the ambipolar, annealing-free, ambient-stable and amorphous properties of these conjugated polymers, the electron-accepting CF_3-BP unit can be considered as a promising building block in preparing the easily processable conjugated polymers used in high-stability optoelectronic applications.

Results and discussion

Synthesis and Characterization

The synthetic routes of the four CF_3-BP-based conjugated polymers (PBPV-TPA, PBPV-CBZ, PBPV-MEH, PBPV-FLO) are outlined in Scheme 1. To minimize the formation of *cis-trans* isomers and structural defects, such as saturated, non-eliminated and tolane-bisbenzyl defects, during Gilch polymerization, which have been proved to be deleterious to the performance of optoelectronic devices,[45] the polymers were prepared by reacting the dimethylenephosphonate of CF_3-BP with the dialdehydes of TPA, CBZ, MEH and FLO via Horner-Emmons polymerization.[46] The reaction was carried out in *N,N*-dimethylformamide (DMF) in the presence of potassium *tert*-butoxide (*t*-BuOK) as base under nitrogen atmosphere at room temperature (see details in the Experimental Section). In order to avoid the end-group effect caused by the aldehyde and methylenephosphonate chain ends, all of the polymers were end-capped with phenyl groups. The repeating units were regarded as respective donor unit (TPA, CBZ, TPA and FLO) at the center, linked by vinylenes then trifluoromethyl-substituted phenyls, as illustrated in Scheme 1. All of the resulted polymers possess moderate number-averaged molecular weights (M_n: 10,000-20,000 g mol^{-1}) with polydispersity indexes (M_w/M_n) of 1.50-1.90, measured by gel permeation chromatography (GPC) with *N,N*-dimethylacetamide (DMAc) as eluent calibrated with polystyrene standards, as shown Table 1. The ^{1}H NMR spectra (Fig. S1-S4) in the ESI further confirm the chemical identity of the four novel CF_3-BP-based conjugated polymers.

Owing to the electrostatic repulsion between the fluorine atoms on trifluoromethyl groups at 2 and 2' positions, the biphenyl units are forced to adapt a non-coplanar conformation. As a result, all of the polymers are organo-soluble, as shown in Table S1. They can be easily dissolved in DMAc, NMP and THF at room temperature. The excellent solubility of polymers leads to the outstanding solution-processability, which is beneficial for device fabrication. The thermal properties of polymers were investigated using differential scanning calorimetry (DSC) and thermogravimetric analysis (TGA). All of the polymers exhibited excellent thermal stabilities with decomposition temperatures higher than 400 °C (5% weight loss under nitrogen atmosphere, as shown in Table 1 and Fig. S5). Owing to the flexibility and rotation-freedom of attached alkyl/alkoxy side chains, the free volume of polymer is generally enhanced. Therefore, glass transition temperatures (T_g) of these polymers decreased with the increasing contents of alkyl/alkoxy side chains. PBPV-FLO with the highest alkyl side chain contents possessed the lowest T_g (125 °C) compared to that of PBPV-TPA (179 °C) which lacked of alkyl/alkoxy side chains.

Journal Name

ARTICLE

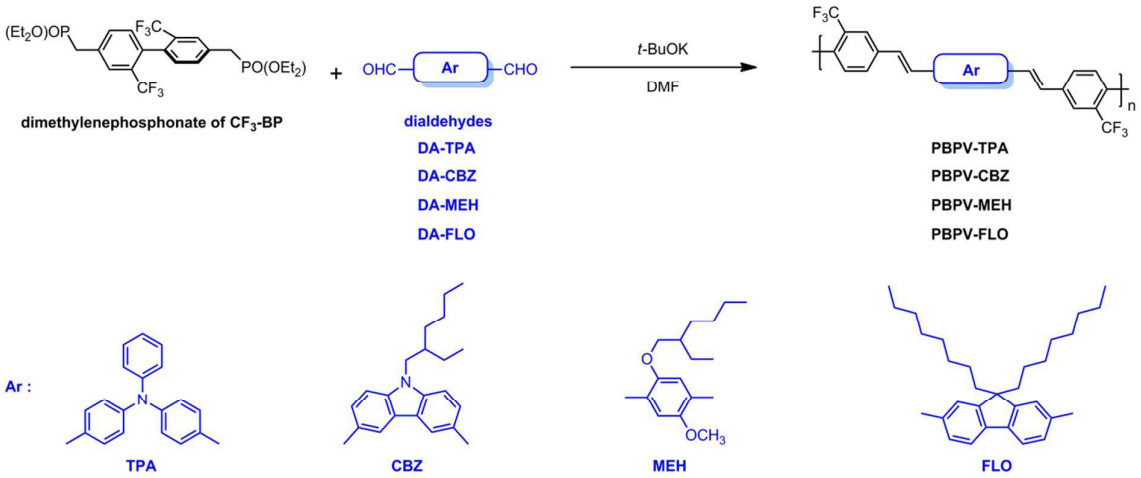

Scheme 1. Synthesis of polymers by Horner-Emmons polymerization.

Table 1. Molecular weight and thermal properties of polymers.

Polymer	M_n [a] [g mol^{-1}]	M_w [a] [g mol^{-1}]	PDI [a]	Yield [%]	T_g [b] [°C]	$T_{d\ 5\%}$ [c] [°C]	Char yield [d] [wt %]
PBPV-TPA	10,000	19,000	1.90	96	179	460	55
PBPV-CBZ	16,000	24,000	1.50	76	170	434	47
PBPV-MEH	17,000	33,000	1.94	85	165	402	50
PBPV-FLO	20,000	35,000	1.75	72	125	436	10

[a] Obtained from GPC using DMAc as solvent and calibrated with polystyrene standards.
[b] Measured by DSC at a heating rate of 20 °C min^{-1} in nitrogen.
[c] Measured by TGA at a heating rate of 10 °C min^{-1} in nitrogen.
[d] Residual weight percentage at 800 °C in nitrogen.

Optical, Electrochemical Properties and Computational Simulation.

UV-vis absorption spectra of dilute polymer solutions in THF (10^{-5} M) and spin-coated thin films on quartz substrates are shown in Fig. 1. The results are summarized in Table 2. The maximum absorption wavelengths of PBPV-TPA, PBPV-CBZ, PBPV-MEH and PBPV-FLO in the dilute solution were 380, 375, 410 and 411 nm, respectively. All polymers showed rather narrow absorption ranging from 300 to 500 nm without the characteristic intramolecular charge transfer (ICT) absorption of the common D-A conjugated polymers.[42, 47] This can be attributed to the non-coplanar backbone conformation and the weaker acceptor property of the CF_3-BP unit. In the case of thin films, maximum absorptions at wavelength λ_{max}= 351, 356, 415 and 390 nm for PBPV-TPA, PBPV-CBZ, PBPV-MEH and PBPV-FLO, respectively, were observed. The maximum absorption of PBPV-MEH in spin-coated thin film was slightly bathochromic-shifted compared to that in the dilute solution. This could be due to the common interchain interaction in the solid state. On the contrary, the hypsochromic-shift in the maximum absorption of the PBPV-TPA, PBPV-CBZ and PBPV-FLO thin films compared to those of their dilute solutions was observed. The hypsochromic-shifted maximum absorption in spin-coated thin films might be due to the H-aggregation of the polymers in the solid state.[48]

Table 2. Optical and electrochemical properties of polymers.

Polymer	Solution λ_{abs} [a)] [nm]	Film λ_{abs} [b)] [nm]	HOMO [c)] [eV]	LUMO [d)] [eV]	E_g [e)] [eV]
PBPV-TPA	380	351	-5.31	-2.86	2.45
PBPV-CBZ	338s, 375 391*s*	356, 411*s*	-5.57	-3.14	2.43
PBPV-MEH	326s, 410	345*s*, 415	-5.72	-3.21	2.51
PBPV-FLO	390, 411	390, 404	-5.80	-3.31	2.49

s: absorption shoulder

[a)] Measured in THF solution with a concentration of 10^{-5} M.

[b)] Measured with polymer spin-coated on quartz substrate.

[c)] $E_{HOMO} = -(E_{onset}^{ox} + 4.80 - 0.09)$ (eV) measured by cyclic voltammetry.

[d)] $E_{LUMO} = -(E_{onset}^{red} + 4.80 - 0.09)$ (eV) measured by cyclic voltammetry.

[e)] E_g = IP (E_{onset}^{ox}) – EA (E_{onset}^{red}) (eV).

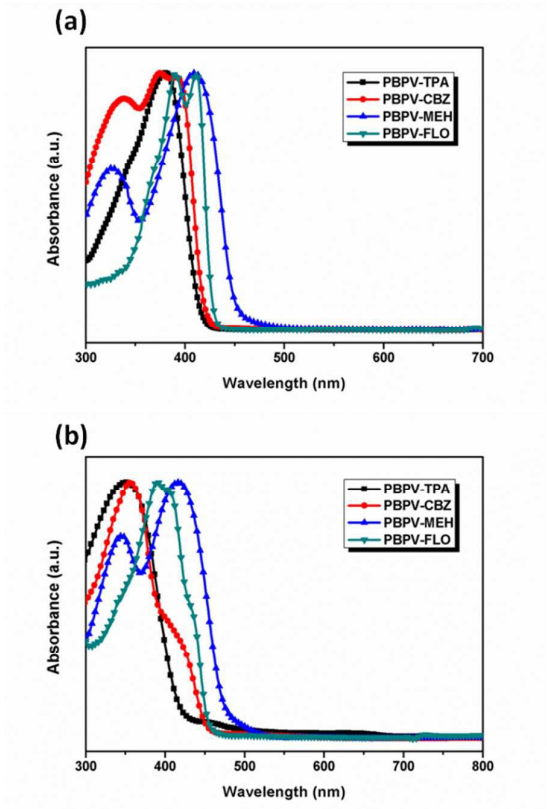

Fig. 1. UV-vis spectra of polymers in (a) dilute THF solution (10^{-5} M) and (b) thin film on quartz plate.

The electrochemical redox properties of the polymers were examined using cyclic voltammetry (CV) with polymer thin films coated on ITO glass. The absolute energy level of ferrocene/ferrocenium (Fc/Fc^+) was assumed to be 4.80 eV below vacuum. The external Fc/Fc^+ redox standard $E_{1/2}$ was measured to be 0.09 V versus Ag/Ag^+ in anhydrous acetonitrile with our CV system. The cyclic voltammograms of the polymers are shown in Fig. 2. The HOMO and LUMO energy levels were translated from their respective oxidation and reduction onset potentials. The calculated HOMO and LUMO energy levels of the polymers are summarized in Table 2. The relatively deeper HOMO and LUMO energy levels of PBPV-TPA, PBPV-CBZ, PBPV-MEH and PBPV-FLO in comparison to their homopolymer analogues and derivatives[49-54] are resulted from the introduction of electron-accepting CF_3-BP. The nearly identical HOMO energy levels of PBPV-MEH (-5.72 eV) and PBPV-FLO (-5.80 eV) indicates the electron-donating abilities of MEH and FLO moieties are in the same level. The stronger electron-donating property of the TPA moieties resulted in the highest-lying HOMO energy level of PBPV-TPA (-5.31 eV) relative to those of the other polymers. The narrower bandgap (E_g) and deeper LUMO energy levels of PBPV-MEH (-3.21 eV) and PBPV-FLO (-3.31 eV) in comparison to those of PBPV-TPA (-2.86 eV) and PBPV-CBZ (-3.14 eV) were contributed to the longer conjugation length from the more linear backbones of PBPV-MEH and PBPV-FLO as shown in the DFT-simulated geometries (Fig. S6). The most bended and non-coplanar backbone geometry resulted from the propeller-shaped TPA units leads to the highest-lying LUMO energy level of PBPV-TPA.

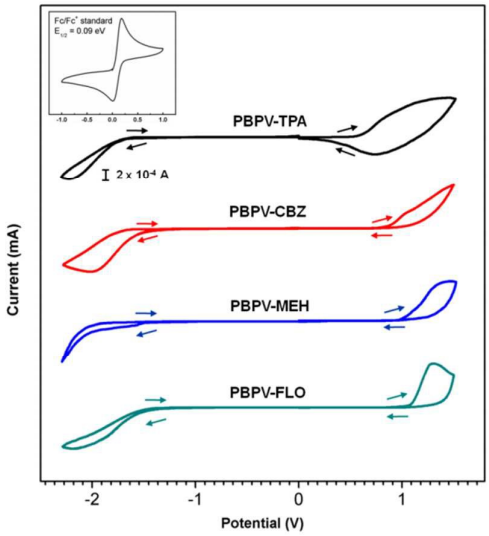

Fig. 2. Cyclic voltammograms of polymers.

To gain further insight into the molecular geometries and electronic features of the polymers, the frontier orbital distributions, HOMOs and LUMOs, of the polymers were calculated by density functional theory (DFT) method. The DFT calculations were conducted on the repeating units of PBPV-TPA, PBPV-CBZ, PBPV-MEH and PBPV-FLO using the B3LYP functional[55] and the 6-31 G** basis set[56] as implemented in GAUSSIAN 09. The repeating units were regarded as respective

donor units at the center, linked by vinylenes then trifluoromethyl-substituted phenyls, as illustrated in Scheme 1. As shown in Fig. 3 and S6, except PBPV-TPA, which contains propeller-shaped TPA moieties, the optimized molecular geometries of the other three repeating units are close to coplanar. More importantly, unlike most D-A copolymers,[57-62] in which the LUMOs are localized at the acceptor units, in the CF_3-BP based conjugated polymers, the HOMO and LUMO distribution contours are all uniformly distributed in the respective repeating units (Fig. 3), except the LUMO of PBPV-TPA. The uniformly delocalized HOMO and LUMO distributions are expected to promote the ambipolarity.[35] The HOMO contour of PBPV-TPA is more evenly distributed than LUMO contour, which may result in the better p-type than n-type characteristic.

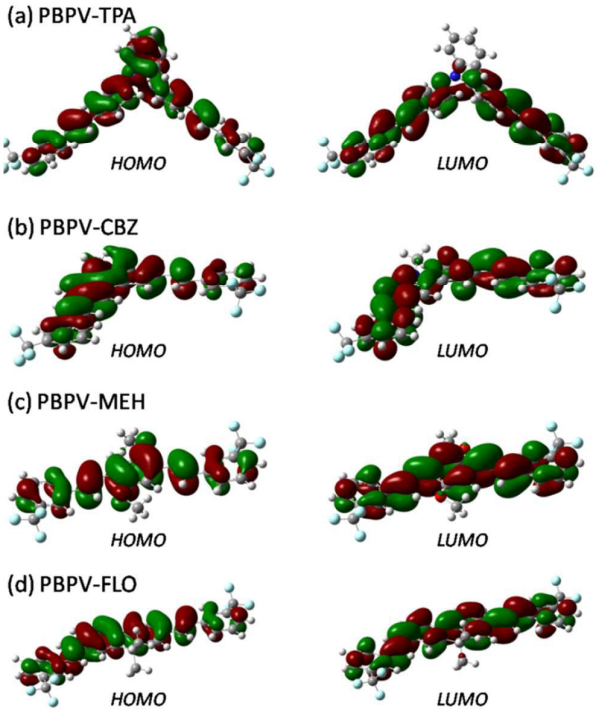

Fig. 3. DFT-simulated geometries and electronic contours of (a) PBPV-TPA, (b) PBPV-CBZ, (c) PBPV-MEH and (d) PBPV-FLO.

Molecular Orientation and Thin-Film Microstructures.

The intermolecular packing and solid-state structures of the active layers are one of the key factors that govern the performance of OFETs. In this regard, thin film morphology and microstructures of these polymers were analyzed by wide-angle x-ray scattering (WAXS), small-angle x-ray scattering (SAXS) and tapping-mode atomic force microscopy (AFM). Fig. 4 and 5 show the WAXS and SAXS curves which were integrated from their 2D ring patterns shown in Fig. S7 and S8, respectively. In our previous study, the CF_3-PBTV, which contains a thiophene core unit in its repeat unit, possesses chain-axis periodicity in its solid-state.[35] In contrast, no diffraction was found in PBPV-TPA, PBPV-CBZ, PBPV-MEH and PBPV-FLO as shown in Fig. 4 and Fig. 5. The lateral side chains on the CBZ, MEH and FLO units, and the propeller geometry of the TPA unit thus hinder the formation of the chain-axis periodicity and make the four conjugated polymers amorphous. To further confirm their amorphous nature, polymers were examined by WAXS after annealed at 120, 180 and 250 °C for 15 min in a temperature-controlled air-circulated oven. The amorphous features of the polymers were found to be independent of the annealing temperatures, as shown in Fig. S9. The annealing-temperature independence of the amorphous polymer thin films is also supported by their relatively smooth morphology revealed by AFM images at the same annealing temperatures as shown in Fig. 6, S10, S11 and S12. No discernible changes were observed after thermal-annealing. Furthermore, no grains or crystalline-like features were detected in the AFM phase images. The root-mean-square (RMS) surface roughness of these polymer thin films was determined to be within 1 nm (0.613-0.875 nm) in the AFM height images, which suggests the smooth surface of the polymer thin films. This phenomenon is in good agreement with the annealing-temperature independent performances of OFETs based on these polymers, as described below.

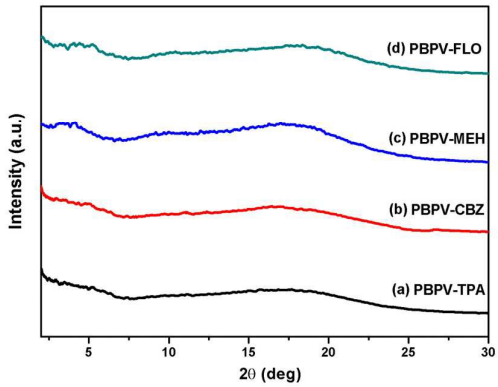

Fig. 4. WAXS patterns of (a) PBPV-TPA, (b) PBPV-CBZ, (c) PBPV-MEH and (d) PBPV-FLO.

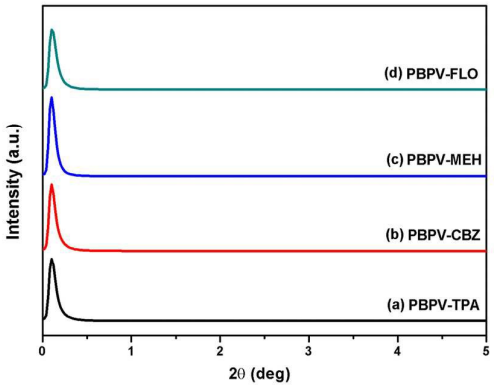

Fig. 5. SAXS patterns of (a) PBPV-TPA, (b) PBPV-CBZ, (c) PBPV-MEH and (d) PBPV-FLO.

OFET Characteristics, Ambient Stability and Annealing-Free Properties.

The OFET characteristics and charge transport properties of these polymers were investigated using the bottom-gate/top-contact device configuration with gold (Au) as electrodes. Thermally-grown SiO_2 (200 nm) and heavily n-doped silicon (n^+-Si) were used as the dielectric insulator (capacitance C_i = 11 nF cm^{-2}) and the gate electrode, respectively. The n-octadecyltrichlorosilane (OTS) self-assembly monolayer was casted onto the SiO_2 dielectric insulator to passivate the SiO_2 surface and prevent electron-trapping OH species. Anhydrous polymer solutions (5 mg L^{-1}) in DMAc were spin-coated (1000 rpm for 30 s) onto the OTS-modified SiO_2 surfaces at room temperature. The thermally-evaporated gold source and drain electrodes were deposited through a shadow mask. The channel length (L) and width (W) were 50 μm and 2000 μm, respectively. All the fabrication processes and characterizations, except SiO_2 growth and gold evaporation, were performed in ambient conditions. The OFET characteristics, including hole mobility (μ_{hole}), electron mobility ($\mu_{electron}$), threshold voltage (V_{th}) and on/off ratio (I_{on}/I_{off}) are shown in Fig. 7, Fig. S13, Table 3 and 4. The ambipolar mobilities of OFETs were extracted from their respective saturation regimes and averaged over 20 devices.

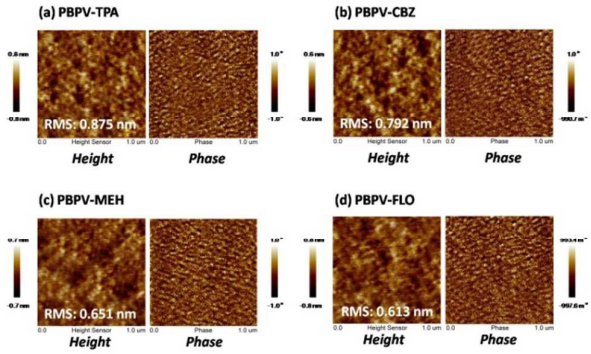

Fig. 6. AFM height and phase images (1 μm × 1 μm) of spin-coated (a) PBPV-TPA, (b) PBPV-CBZ, (c) PBPV-MEH and (d) PBPV-FLO films on OTS-modified SiO_2/Si substrates.

As summarized in Table 3, OFETs based on these polymers exhibited typical ambipolar transfer and output characteristics with well-balanced hole (μ_{hole}) and electron ($\mu_{electron}$) mobilities in ambient conditions. PBPV-FLO exhibited the highest hole mobility of 0.0152 cm^2 V^{-1} s^{-1} and electron mobility of 0.0120 cm^2 V^{-1} s^{-1}. Compared to those of PBPV-FLO and PBPV-MEH, the relatively low hole and electron mobilities (in the magnitude of 10^{-3}) of PBPV-TPA and PBPV-CBZ might be due to their more bended backbones as shown from the results of DFT calculation and UV-vis absorption spectra. The transfer characteristics of all the devices performed negligible hysteresis suggesting the low contents of charge-transporting traps in the interface between active layer and dielectric insulator. The well-balanced ambipolar OFET characteristics, as depicted in the transfer and output curves in Fig. 7 and Fig. S13, might be due to the unique match of donors and CF_3-BP acceptor. TPA-, CBZ- MEH- and FLO-based conjugated polymers are generally classified as p-type semiconductors. Moreover, OFET characteristic remained to be p-type even when strong acceptor, such as isoindigos, benzothiadiazoles, diketopyrrolopyrroles, were incorporated in the polymer backbone.[42-44] Therefore, it is worth mentioning that trifluoromethyl-containing CF_3-BP could be one of the potential acceptor building blocks for the lately developed donors, such as naphthobisthiadiazole,[36] benzodi(cyclopentadithiophene)[37] and indacenodiselenophene,[38] for the future investigation of high performance ambipolar OFETs. As shown in Fig. 7 and Fig. S13, the smooth and non-s-shaped linear regimes for both p- and n-channel in output characteristics reveal the comparatively low contact resistance at the active layer/dielectric insulator interface.

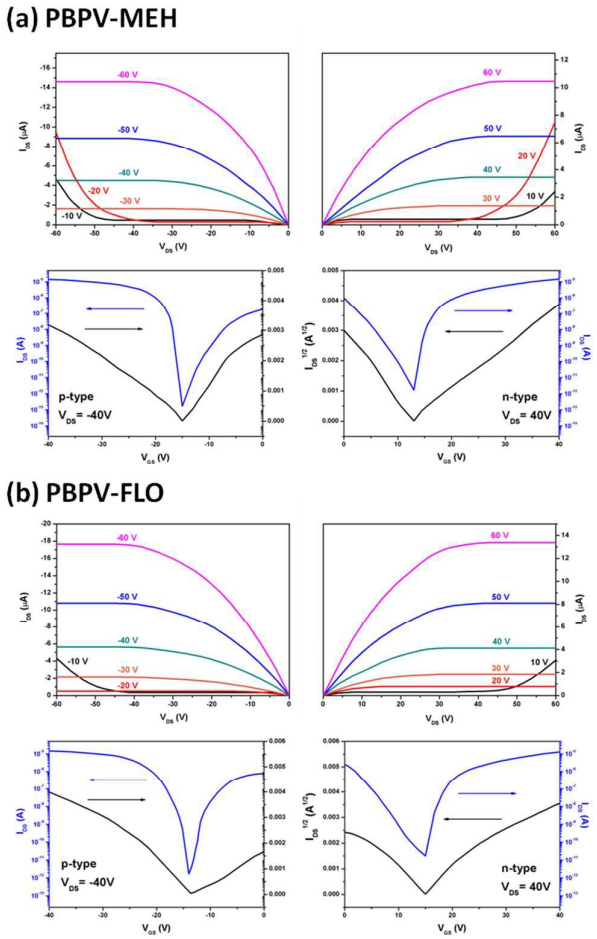

Fig. 7. Ambipolar output and transfer characteristics of OFET based on (a) PBPV-MEH and (b) PBPV-FLO.

Table 3. OFET characteristics and ambient stability of polymers.

Polymer	Channel	As-fabricated			30-Day[b]			90-Day[b]		
		Mobility[a] [$cm^2 V^{-1}s^{-1}$]	V_{th} [V]	I_{on}/I_{off}	Mobility[a] [$cm^2 V^{-1}s^{-1}$]	V_{th} [V]	I_{on}/I_{off}	Mobility[a] [$cm^2 V^{-1}s^{-1}$]	V_{th} [V]	I_{on}/I_{off}
PBPV-TPA	*p*	0.0075	-13	10^5	0.0070	-15	10^5	0.0065	-15	10^4
	n	0.0043	11	10^6	0.0042	11	10^5	0.0038	13	10^5
PBPV-CBZ	*p*	0.0053	-15	10^4	0.0051	-15	10^4	0.0047	-17	10^4
	n	0.0068	14	10^5	0.0064	15	10^5	0.0059	16	10^5
PBPV-MEH	*p*	0.0131	-15	10^6	0.0128	-16	10^6	0.0123	-17	10^5
	n	0.0086	13	10^6	0.0082	15	10^6	0.0080	15	10^5
PBPV-FLO	*p*	0.0152	-14	10^6	0.0147	-16	10^6	0.0145	-17	10^6
	n	0.0120	15	10^6	0.0117	16	10^6	0.0113	18	10^5

[a] Mobilities were calculated using equation $\mu = 2I_{DS}L\,[C_i W(V_{GS}-V_{th})^2]^{-1}$.
(μ = mobility, L = length, C_i = Capacitance, W = width, V_{th} = threshold voltage).
[b] Long-term stability of OFET was investigated under ambient conditions.

Table 4. OFET characteristics with various annealing temperatures.

Polymer	Channel	Annealed at 120 °C[a]			Annealed at 180 °C[a]			Annealed at 250 °C[a]		
		Mobility[a] [$cm^2 V^{-1}s^{-1}$]	V_{th} [V]	I_{on}/I_{off}	Mobility[a] [$cm^2 V^{-1}s^{-1}$]	V_{th} [V]	I_{on}/I_{off}	Mobility[a] [$cm^2 V^{-1}s^{-1}$]	V_{th} [V]	I_{on}/I_{off}
PBPV-TPA	*p*	0.0075	-14	10^5	0.0074	-15	10^5	0.0070	-16	10^5
	n	0.0042	13	10^6	0.0040	12	10^4	0.0039	13	10^4
PBPV-CBZ	*p*	0.0051	-15	10^4	0.0052	-15	10^4	0.0051	-16	10^4
	n	0.0065	15	10^5	0.0065	15	10^4	0.0063	15	10^4
PBPV-MEH	*p*	0.0125	-15	10^6	0.0123	-15	10^6	0.0120	-16	10^5
	n	0.0080	15	10^6	0.0080	15	10^6	0.0075	16	10^5
PBPV-FLO	*p*	0.0148	-15	10^6	0.0148	-15	10^6	0.0144	-16	10^5
	n	0.0115	16	10^6	0.0112	15	10^6	0.0105	16	10^5

[a] OFETs were thermally annealed on a temperature-controlled hot plate for 15 min under ambient conditions.

Among the OFETs, remarkably high on/off ratios of 10^6 for both p- and n-channel were obtained from devices based on PBPV-MEH and PBPV-FLO, as summarized in Table 3. In comparison with the on/off ratios of ambipolar OFETs based on low-bandgap (0.96-1.87 eV) conjugated polymers, the relatively high on/off ratios of OFETs based on PBPV-MEH and PBPV-FLO might be due to their comparatively large bandgaps. The high on/off ratios are attributed to the reduced off-current leakage by large bandgaps and excluded detrimental oxygen-doping processes by deep HOMO energy levels.[63]

As OFETs are now close to practical applications, the issues regarding the reliability in ambient conditions have to be addressed. As provided in Fig. 8 and Table 3, the characteristics of OFETs remained nearly unchanged in ambient conditions up to 90 days. All of the charge mobilities were marginally decreased within 0.001 $cm^2 V^{-1} s^{-1}$ for both p- and n-channels. The performance degradation of bottom-gate OFETs without encapsulation in ambient conditions was believed to be caused by the diffusion of moistures and oxygen from the surface of active layers.[64] Therefore, the remarkable ambient stability of OFETs based on these polymers could be resulted from the better resistance to the diffusion of moisture by the enhanced hydrophobicity of fluorine atoms on the CF_3-BPs. Moreover, the enhanced oxidative stability from the relatively deep HOMO energy levels (-5.31 to -5.80 eV), which are resulted from the insertion of electron-accepting

trifluoromethyl-substituted CF_3-BPs, might also contribute to the superior ambient stability. The stability of ambipolar and amorphous OFETs based on polymers containing TPA, CBZ, MEH and FLO as donors in ambient conditions has never been examined. In this study, the ambient stability of these ambipolar amorphous OFETs is demonstrated for the first time. The ambient stability of PBPV-TPA, PBPV-CBZ, PBPV-MEH and PBPV-FLO might lead to a more efficient device fabrication in the relatively uncritical environment with simplified encapsulation.

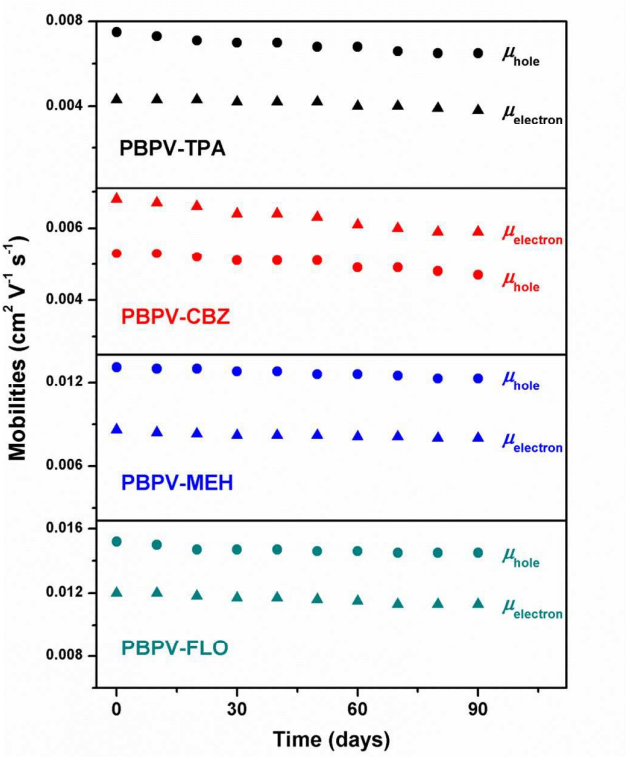

Fig. 8. Ambient stability of OFETs based on PBPV-TPA, PBPV-CBZ, PBPV-MEH and PBPV-FLO.

Since most of the charge transport in OFET was reported to be strongly influenced by the molecular orientation and thin film morphology,[17-19] polymer backbone aligning processes through thermal annealing are considered a necessity to achieve high device performance. For example, post thermal treatment were reported to sufficiently induce morphological changes in poly(3-hexylthiophene) thin films, which led to significant variation of their OFET performances.[65] The hole and electron mobilities were found to be around 10-fold higher for the OFET based on a benzodipyrorolidone-containing conjugated polymer after thermal annealing at 250 °C.[66] The similar trend after thermal annealing was also found on a naphthalene-based OFET.[67] In this regard, OFETs based on PBPV-TPA, PBPV-CBZ, PBPV-MEH and PBPV-FLO were thermally annealed at various temperatures (120, 180 and 250 °C) for 15 min on a temperature-controlled hot plate. OFET characteristics, including ambipolar mobilities, threshold voltages and on/off ratios, remained almost identical after thermal annealing, as shown in Table 4. The annealing-temperature-independent characteristics of the OFETs are believed to be ascribed to the unchanged morphology and molecular orientation of the polymers after thermal annealing. Therefore, OFETs based on these polymers can function without considering the molecular orientation and morphological issues, which creates consistent OFET performances regardless the fabrication processes. In other words, highest mobilities were achieved, once the devices are fabricated without further time-consuming thermal annealing. Such invulerability in film morphology and molecular orientation to temperature not only improves the thermal stability of devices during operation, but enhances the fabrication reproducibility and simplicity as well. Thus, CF_3-BP could be a promising acceptor for the lately-developed high mobility donors to achieve annealing-free and ambient-stable OFETs with ambipolarity and high performance.

Conclusion

We have successfully synthesized four novel conjugated polymers, PBPV-TPA, PBPV-CBZ, PBPV-MEH and PBPV-FLO, consisting of CF_3-BP as the acceptor with various donors (TPA, CBZ, MEH and FLO). The polymers show good solution-processability in common organic solvents. Their amorphous structures, which were confirmed by WAXS, SAXS and AFM, are attributed to lateral side chains on the CBZ, MEH and FLO units, and the propeller geometry of the TPA unit. By the integration of CF_3-BPs, the ambipolarities with well-balanced charge mobilities were successfully introduced to the p-type TPA, CBZ, MEH and FLO materials. OFET based on PBPV-FLO exhibits the highest hole mobility of 0.0152 cm^2 V^{-1} s^{-1} and electron mobility of 0.0120 cm^2 V^{-1} s^{-1}. Through the introduction of CF_3-BPs, annealing-free, amorphous ambipolar OFETs are realized. OFETs based on these polymers also demonstrate outstanding ambient stability. Their performances remain nearly unchanged after stored in ambient conditions for 90 days without encapsulation. This could be attributed to the enhanced oxidative stability from their relatively deep HOMO energy levels and better resistance to moistures from their trifluoromethyl substitution. Though the hole and electron mobilities of these polymers are not as high as the state-of the-art records (10-0.1 cm^2 V^{-1} s^{-1}) of recently-developed materials, the multiple functions, including balanced ambipolarity, amorphous, ambient-stable and annealing-free characteristics, induced by CF_3-BP unit demonstrated its potential as an efficient acceptor building block. With careful selection of the high-performance donor units, OFETs with high ambipolar mobilities and ambient-stable, annealing-free characteristics might be realized based on CF_3-BP unit.

Experimental

General Tetrabutylammonium perchlorate (TBAP) used in cyclic voltammetric measurements was recrystallized twice with

ethyl acetate and dried at 120 °C under reduced pressure for 48 h. All of the other reagents were purchased from commercial companies and used as received. All of the solvents used were purified according to standard method prior to use. All melting points were determined on a Mel-Temp capillary melting point apparatus. ^{1}H NMR and ^{13}C NMR spectra were measured at 500 and 125 MHz on a Bruker Avance-500 spectrometer, respectively, using $CDCl_3$ and DMSO-d_6 as solvent and tetramethylsilane (TMS) as internal standard. Elemental analyses were performed on Heraeus Vario analyzer. Number-average (M_n) and weight-average (M_w) molecular weights of polymers were measured on a JASCO GPC system (PU-980) equipped with an RI detector (RI-930), a Jordi Gel DVB Mixed Bed column (250 mm x 10 mm) column, using *N,N*-dimethylacetamide (DMAc) as the eluent and calibrated with polystyrene standards. Thermogravimetric analysis (TGA) was performed with a TA TGA Q500 thermogravimetric analyzer using a heating rate of 10 °C min^{-1} under N_2 atmosphere. Differential scanning calorimetry (DSC) measurements were carried out under N_2 atmosphere using a PerkineElmer DSC 4000 analyzer at a heating rate of 20 °C min^{-1}. UV-Vis spectrometry was carried out on a JASCO V-670 UV-Vis/NIR spectrophotometer. Cyclic voltammetric (CV) measurements were carried out on a CH Instrument 611C electrochemical analyzer at room temperature in a three-electrode electrochemical cell with a working electrode (polymer film coated on ITO glass), a reference electrode (Ag/Ag^+, referenced against ferrocene/ferrocenium (Fc/Fc^+), 0.09 V), and a counter electrode (Pt gauze) at a scan rate of 100 mV s^{-1}. CV measurements for polymer films were performed in an electrolyte solution of 0.1 M tetrabutylammonium perchlorate (TBAP) in anhydrous acetonitrile. The potential window at oxidative scan and reductive scan was 0~1.5 V and 0~-2.4 V, respectively. The HOMO energy levels were calculated from the equation $E_{HOMO} = -(E_{onset}^{ox} + 4.80 - 0.09)$ (eV). The LUMO energy levels were calculated from the equation $E_{LUMO} = -(E_{onset}^{red} + 4.80 - 0.09)$ (eV).[68] Density functional theory (DFT) calculations were performed using the B3LYP functional[55] and the 6-31 G** basis set[56] as implemented in GAUSSIAN 09. The wide-angle x-ray scattering (WAXS) and small-angle x-ray scattering (SAXS) powder patterns were performed on a Bruker AXS GmbH / NANOSTAR U diffractometer operated at a voltage of 50 kV and a current of 50 mA with Cu Kα radiation (λ = 1.542 Å) using a FLA 7000 image plate and Vantec-2000 detector, respectively. Polymer powders were thermally annealed in an temperature-controlled air-circulated oven under ambient conditions for the annealing-temperature-independent measurement.

Organic field-effect transistor fabrication and characterization All fabrication processes, except SiO_2 growth and gold evaporation, were performed in ambient conditions in a conventional hood. OFET devices were fabricated with a bottom-gate, top-contact configuration. Thin conjugated polymer thin films were deposited by spin-coasting at 1000 rpm for 30 sec onto n-octadecyltrichlorosilane (OTS)-modified heavily doped n^+-Si wafer with thermally grown SiO_2 dielectric layer (200 nm). The polymer solution was (5 mg mL^{-1}) was prepared in anhydrous DMAc and filtered through a 0.22 μm syringe filter. The capacitance of SiO_2 gate insulator was 11 nF cm^{-2}. Prior to the treatment of OTS, the wafers were sonication-cleaned by acetone and isopropanol, sequentially, and were then dried at 100 °C for 10 min in vacuum oven. The source and drain electrode were obtained by thermally evaporated gold (Au, 30 nm) through a shadow mask. The channel width (W) and length (L) were 2000 and 50 μm, respectively. All the OFET characteristics were measured with a Keithley 4200-SCS semiconductor characterization system at room temperature in ambient conditions. Key device parameters, such as charge mobilities (μ) and on/off ratio (I_{on}/I_{off}) were obtained from the source-drain current (I_{DS}) versus gate-source voltage (V_{GS}) characteristics employing standard procedures. Mobilities were extracted from the formula defined by saturation regime in transfer plots, $\mu = 2I_{DS}L\,[C_iW(V_{GS}-V_{th})^2]^{-1}$, where V_{th} is the threshold voltage. Threshold voltage was obtained from the intercept of V_{GS} versus $I_{DS}^{1/2}$ plots. OFETs were stored under ambient conditions for 90 days in a conventional hood for the long-term ambient stability measurement. OFETs were thermally annealed on a temperature-controlled hot plate under ambient conditions in a conventional hood for the annealing-temperature-independent measurement.

Monomer synthesis 2,2'-Bis(trifluoromethyl)-4,4'-bis(diethyl methylenephosphonate)biphenyl (dimethylenephosphonate of CF3-BP) was synthesized through an eight-step synthetic route according to our previous publication as shown in the ESI.[35] 4,4'-Diformyltriphenylamine (DA-TPA), 9-(2-ethylhexyl)-3,6-diformylcarbazole (DA-CBZ), 2-(2-ethylhexyloxy)-5-methoxybenzene-1,4-dicarbaldehyde (DA-MEH) and 9,9-dioctylfluorene-2,7-dicarbaldehyde (DA-FLO) were synthesized as described in the ESI according to the procedures published in literature.

Polymer synthesis

PBPV-TPA To a 100-mL, three-necked, round-bottomed flask were added dimethylenephosphonate of CF_3-BP (0.27 g, 0.46 mmol), DA-TPA (0.14 g, 0.46 mmol) and anhydrous DMF (21.00 mL). 1.0 M *t*-BuOK (4.00 mL, 4.00 mmol, in THF solution) was slowly added with a syringe at room temperature under nitrogen atmosphere. The reaction mixture was further stirred at room temperature for 48 h under nitrogen atmosphere. Benzaldehyde (0.01 mL, 0.1 mmol) was added to the mixture. 1.0 M *t*-BuOK (0.5 mL, 0.5 mmol, in THF solution) was slowly added with a syringe. After the reaction was stirred for 6 h, diethyl benzylphosphonate (0.02 mL, 0.1 mmol) was added to the mixture. 1.0 M *t*-BuOK (0.5 mL, 0.5 mmol, in THF solution) was slowly added with a syringe and the reaction was further stirred for 6 h. The reaction mixture was then poured into water. The precipitate that formed was collected by filtration and washed with hot methanol (Soxhlet apparatus) for 24 h

and dried at 100 °C overnight under reduced pressure to afford 0.32 g of light-yellow solids (yield: 96%). ^{1}H NMR (500 MHz, DMSO-d_6, δ, ppm): 8.00 (s, 2H; H_c), 7.86 (s, 2H; H_b), 7.72 (s, 4H; H_f), 7.48 (dd, 2H; H_i), 7.38 (s, 2H; H_a), 7.33 (s, 1H; H_j), 7.24 (s, 2H; H_h), 7.18 (s, 2H; H_d), 7.12 (s, 4H; H_g), 6.95 (s, 2H; H_e), as shown in Fig. S1; Anal. Calcd. for $C_{36}H_{23}F_6N$: C 74.08, H 3.97, N 2.40; found: C 72.13, H 2.99, N 2.01.

PBPV-CBZ To a 100-mL, three-necked, round-bottomed flask were added dimethylenephosphonate of CF_3-BP (0.34 g, 0.58 mmol), DA-CBZ (0.19 g, 0.58 mmol) and anhydrous DMF (27.00 mL). 1.0 M *t*-BuOK (5.00 mL, 5.00 mmol, in THF solution) was slowly added with a syringe at room temperature under nitrogen atmosphere. The reaction mixture was further stirred at room temperature for 48 h under nitrogen atmosphere. Benzaldehyde (0.01 mL, 0.1 mmol) was added to the mixture. 1.0 M *t*-BuOK (0.5 mL, 0.5 mmol, in THF solution) was slowly added with a syringe. After the reaction was stirred for 6 h, diethyl benzylphosphonate (0.02 mL, 0.1 mmol) was added to the mixture. 1.0 M *t*-BuOK (0.5 mL, 0.5 mmol, in THF solution) was slowly added with a syringe and the reaction was further stirred for 6 h. The reaction mixture was then poured into water. The precipitate that formed was collected by filtration and washed with hot methanol (Soxhlet apparatus) for 24 h and dried at 100 °C overnight under reduced pressure to afford 0.50 g of light-yellow solids (yield: 76%). ^{1}H NMR (500 MHz, DMSO-d_6, δ, ppm): 8.10 (s, 2H; H_c), 7.92 (s, 2H; H_b), 7.73-7.78 (m, 4H; H_h & H_d), 7.35 (s, 2H; H_a), 7.21 (s, 2H; H_f), 7.17 (s, 2H; H_e), 7.07 (s, 2H; H_g), 4.43 (s, 2H; H_i), 2.03 (m, 1H; H_j), 1.15-1.38 (m, 8H; H_k, H_m, H_n, H_o), 0.75-0.86 (m, 6H; H_l, H_p) , as shown in Fig. S2; Anal. Calcd. for $C_{40}H_{37}F_6N$: C 74.39, H 5.78, N 2.17; found: C 73.25, H 5.22, N 1.98.

PBPV-MEH To a 100-mL, three-necked, round-bottomed flask were added dimethylenephosphonate of CF_3-BP (0.17 g, 0.30 mmol), DA-MEH (0.09 g, 0.30 mmol) and anhydrous DMF (15.20 mL). 1.0 M *t*-BuOK (2.30 mL, 2.30 mmol, in THF solution) was slowly added with a syringe at room temperature under nitrogen atmosphere. The reaction mixture was further stirred at room temperature for 48 h under nitrogen atmosphere. Benzaldehyde (0.01 mL, 0.1 mmol) was added to the mixture. 1.0 M *t*-BuOK (0.5 mL, 0.5 mmol, in THF solution) was slowly added with a syringe. After the reaction was stirred for 6 h, diethyl benzylphosphonate (0.02 mL, 0.1 mmol) was added to the mixture. 1.0 M *t*-BuOK (0.5 mL, 0.5 mmol, in THF solution) was slowly added with a syringe and the reaction was further stirred for 6 h. The reaction mixture was then poured into water. The precipitate that formed was collected by filtration and washed with hot methanol (Soxhlet apparatus) for 24 h and dried at 100 °C overnight under reduced pressure to afford 0.15 g of orange solids (yield: 85%). ^{1}H NMR (500 MHz, DMSO-d_6, δ, ppm): 7.97 (d, 2H; H_c), 7.82 (s, 2H; H_b), 7.51 (d, 2H; H_d), 7.30 (s, 2H; H_a), 7.20 (s, 2H; H_e), 7.00 (s, 2H; H_f), 3.89 (d, 2H; H_h), 3.82 (s, 3H; H_g), 1.70 (m, 1H; H_i), 1.23-1.42 (m, 8H; H_j, H_k, H_l, H_n), 0.84 (m, 6H; H_m & H_o), as shown in Fig. S3; Anal. Calcd. for $C_{33}H_{32}F_6O_2$: C 68.96, H 5.62; found: C 66.85, H 4.57.

PBPV-FLO To a 100-mL, three-necked, round-bottomed flask were added dimethylenephosphonate of CF_3-BP (0.17 g, 0.30 mmol), DA-FLO (0.13 g, 0.30 mmol) and anhydrous DMF (15.20 mL). 1.0 M *t*-BuOK (2.30 mL, 2.30 mmol, in THF solution) was slowly added with a syringe at room temperature under nitrogen atmosphere. The reaction mixture was further stirred at room temperature for 48 h under nitrogen atmosphere. Benzaldehyde (0.01 mL, 0.1 mmol) was added to the mixture. 1.0 M *t*-BuOK (0.5 mL, 0.5 mmol, in THF solution) was slowly added with a syringe. After the reaction was stirred for 6 h, diethyl benzylphosphonate (0.02 mL, 0.1 mmol) was added to the mixture. 1.0 M *t*-BuOK (0.5 mL, 0.5 mmol, in THF solution) was slowly added with a syringe and the reaction was further stirred for 6 h. The reaction mixture was then poured into water. The precipitate that formed was collected by filtration and washed with hot methanol (Soxhlet apparatus) for 24 h and dried at 100 °C overnight under reduced pressure to afford 0.15 g of light-yellow solids (yield: 72%). ^{1}H NMR (500 MHz, DMSO-d_6, δ, ppm): 8.25 (s, 2H; H_f), 8.16 (s, 2H; H_c), 8.03 (s, 2H; H_b), 7.79 (s, 2H; H_d), 7.62-7.71 (m, 4H; H_g & H_h), 7.44 (s, 2H; H_a), 7.17 (s, 2H; H_e), 2.09 (m, 4H; H_i), 1.21-1.38 (m, 20H; H_k, H_l, H_m, H_n, H_o), 0.80 (s, 6H; H_p), 0.55-0.61 (m, 4H; H_j), as shown in Fig. S4; Anal. Calcd. for $C_{47}H_{50}F_6$: C 77.43, H 6.92; found: C 75.29, H 6.00.

Notes and references

1 K.-J. Baeg, M. Caironi, Y.-Y. Noh, *Adv. Mater.,* 2013, **25**, 4210.
2 H.-C. Wu, C.-L. Liu, W.-C. Chen, *Polym. Chem.,* 2013, **4**, 5261.
3 H. Li, F. S. Kim, G. Ren, S. A. Jenekhe, *J. Am. Chem. Soc.,* 2013, **135**, 14920.
4 E. J. Meijer, D. M. de Leeuw, S. Setayesh, E. van Veenendaal, B. H. Huisman, P. W. M. Blom, J. C. Hummelen, U. Scherf, T. M. Klapwijk, *Nat. Mater.,* 2003, **2**, 678.
5 I. McCulloch, R. S. Ashraf, L. Biniek, H. Bronstein, C. Combe, J. E. Donaghey, D. I. James, C. B. Nielsen, B. C. Schroeder, W. Zhang, *Acc. Chem. Res.,* 2012, **45**, 714.
6 C. Wang, H. Dong, W. Hu, Y. Liu, D. Zhu, *Chem. Rev.,* 2012, **112**, 2208.
7 J.-M. Jiang, H.-K. Lin, Y.-C. Lin, H.-C. Chen, S.-C. Lan, C.-K. Chang, K.-H. Wei, *Macromolecules,* 2014, **47**, 70.
8 J. Terao, A. Wadahama, A. Matono, T. Tada, S. Watanabe, S. Seki, T. Fujihara, Y. Tsuji, *Nat. Commun.,* 2013, **4**, 1691.
9 J. Lee, A. R. Han, H. Yu, T. J. Shin, C. Yang, J. H. Oh, *J. Am. Chem. Soc.,* 2013, **135,** 9540.
10 J. Liu, R. Zhang, G. Sauvé, T. Kowalewski, R. D. McCullough, *J. Am. Chem. Soc.,* 2008, **130**, 13167.
11 C. M. Amb, M. R. Craig, U. Koldemir, J. Subbiah, K. R. Choudhury, S. A. Gevorgyan, M. Jørgensen, F. C. Krebs, F. So, J. R. Reynolds, *ACS Appl. Mater. Interfaces,* 2012, **4**, 1847.
12 F. C. Krebs, K. Norrman, *ACS Appl. Mater. Interfaces,* 2010, **2**, 877.
13 Z. Bao , A. Dodabalapur , A. J. Lovinger, *Appl. Phys. Lett.,* 1996, **69**, 4108.
14 C. Luo, A. K. K. Kyaw, L. A. Perez, S. Patel, M. Wang, B. Grimm, G. C. Bazan, E. J. Kramer, A. J. Heeger , *Nano Lett.*, 2014, **14**, 2764.
15 Z. Chen, M. J. Lee, R. S. Ashraf, Y. Gu, S. Albert-Seifried, M. M. Nielsen, B. Schroeder, T. D. Anthopoulos, M. Heeney, I. McCulloch and H. Sirringhaus, *Adv. Mater.*, 2012, **24**, 647.

16 C. B. Nielsen, M. Turbiez, I. McCulloch, *Adv. Mater.*, 2013, **25**, 1859.
17 R. Noriega, J. Rivnay, K. Vandewal, F. P. V. Koch, N. Stingelin, P. Smith, M. F. Toney, A. Salleo, *Nat. Mater.,* 2013, 12, 1038.
18 T. Schuettfort, B. Watts, L. Thomsen, M. Lee, H. Sirringhaus, C. R. McNeill, *ACS Nano,* 2012, **6**, 1849.
19 A. Saeki, Y. Koizumi, T. Aida, S. Seki, *Acc. Chem. Res.,* 2012, **45**, 1193.
20 M. M. Islam, S. Pola, Y.-T. Tao, *ACS Appl. Mater. Interfaces,* 2011, **3**, 2136.
21 K. C. Dickey, J. E. Anthony, Y. L. Loo, *Adv. Mater.,* 2006, **18**, 1721.
22 Q. Bao, J. Li, C. M. Li, Z. L. Dong, Z. Lu, F. Qin, C. Gong, J. Guo, *J. Phys. Chem. B,* 2008, **112**, 12270.
23 A. Zen, J. Pflaum, S. Hirschmann, W. Zhuang, F. Jaiser, U. Asawapirom, J. P. Rabe, U. Scherf, D. Neher, *Adv. Funct. Mater.,* 2004, **14**, 757.
24 C. Kanimozhi, N. Yaacobi-Gross, K. W. Chou, A. Amassian, T. D. Anthopoulos, S. Patil, *J. Am. Chem. Soc.,* 2012, **134**, 16532.
25 C. B. Nielsen, M. Turbiez, I. McCulloch, *Adv. Mater.,* 2013, ***25***, 1859.
26 T. Lei, J.-Y. Wang, J. Pei, *Acc. Chem. Res.,* 2014, **47**, 1117.
27 H. Yan, Z. Chen, Y. Zheng, C. Newman, J. R. Quinn, F. Dotz, M. Kastler, A. Facchetti, *Nature,* 2009, **457**, 679.
28 X. Zhan, A. Facchetti, S. Barlow, T. J. Marks, M. A. Ratner, M. R. Wasielewski, S. R. Marder, *Adv. Mater.,* 2011, **23**, 268.
29 M. L. Tang, Z. Bao, *Adv. Mater.,* 2011, **23**, 446.
30 O. Knopfmacher, M. L. Hammock, A. L. Appleton, G. Schwartz, J. Mei, T. Lei, J. Pei, Z. Bao, *Nat. Commun.,* 2014, **5**, 2954.
31 S. C. Price, A. C. Stuart, L. Yang, H. Zhou, W. You, *J. Am. Chem. Soc.,* 2011, **133**, 4625.
32 N. Wang, Z. Chen, W. Wei, Z. Jiang, *J. Am. Chem. Soc.,* 2013, **135**, 17060.
33 B. Lim, K.-J. Baeg, H.-G. Jeong, J. Jo, H. Kim, J.-W. Park, Y.-Y. Noh, D. Vak, J.-H. Park, J.-W. Park, D.-Y. Kim, *Adv. Mater.,* 2009, **21**, 2808.
34 T. Lei, J.-H. Dou, Z.-J. Ma, C.-H. Yao, C.-J. Liu, J.-Y. Wang, J. Pei, *J. Am. Chem. Soc.,* 2012, **134**, 20025.
35 C.-J. Chiang, J.-C. Chen, H.-Y. Tsao, K.-Y. Wu, C.-L. Wang, *Adv. Funct. Mater.,* 2015, **25**, 606.
36 I. Osaka, M. Shimawaki, H. Mori, I. Doi, E. Miyazaki, T. Koganezawa, K. Takimiya, *J. Am. Chem. Soc.,* 2012, **134**, 3498.
37 Y.-L. Chen, C.-Y. Chang, Y.-J. Cheng, C.-S. Hsu, *Chem. Mater.,* 2012, **24**, 3964.
38 H.-H. Chang, C.-E. Tsai, Y.-Y. Lai, W.-W. Liang, S.-L. Hsu, C.-S. Hsu, Y.-J. Cheng, *Macromolecules,* 2013, **46**, 7715.
39 Y. Zhu, A. Babel, S. A. Jenekhe, *Macromolecules,* 2005, ***38,*** 7983.
40 J.-C. Chen, H.-C. Wu, C.-J. Chiang, T. Chen, L. Xing, *J. Mater. Chem. C,* 2014, **2**, 4835.
41 Z. Chen, J. Fang, F. Gao, T. J. K. Brenner, K. K. Banger, X. Wang, W. T. S. Huck, H. Sirringhaus, *Org. Electron.,* 2011, **12**, 461.
42 Y. Koizumi, M. Ide, A. Saeki, C. Vijayakumar, B. Balan, M. Kawamoto, S. Seki, *Polym. Chem.,* 2013, **4**, 484.
43 J.-H. Kim, H. U. Kim, I.-N. Kang, S. K. Lee, S.-J. Moon, W. S. Shin, D.-H. Hwang, *Macromolecules,* 2012, **45**, 8628.
44 F. Liu, C. Wang, J. K. Baral, L. Zhang, J. J. Watkins, A. L. Briseno, T. P. Russell, *J. Am. Chem. Soc.,* 2013, **135**, 19248.
45 A. Fleissner, K. Stegmaier, C. Melzer, H. von Seggern, T. Schwalm, M. Rehahn, *Chem. Mater.,* 2009, **21**, 4288.
46 H.-H. Hörhold, M. Helbig, D. Raabe, J. Opfermann, U. Scherf, R. Stockmann, D. Weiß, *Z. Chem.*, 1987, **27**, 126.
47 D. Mori, H. Benten, I. Okada, H. Ohkita, S. Ito, *Adv. Energy Mater.* 2014, **4**, 1301006.
48 A. Eisfeld, J. S. Briggs, *Chem. Phys.,* 2006, **324**, 376.
49 J. N. de Freitas, R. W. C. Li, A. F. Nogueira, J. Gruber, *Mater. Chem. Phys.,* 2011, **130**, 223.
50 C. Deng, P. Gong, Q. He, J. Cheng, C. He, L. Shi, D. Zhu, T. Lin, *Chem. Phys. Lett.,* 2009, **483**, 219.
51 V. Gowrishankar, S. R. Scully, M. D. McGehee, Q. Wang, H. M. Branz, *Appl. Phys. Lett.,* 2006, **89**, 252102.
52 M. Grigoras, A. M. Catargiu, T. Ivan, L. Vacareanu, B. Minaev, E. Stromylo, *Dyes Pigm.,* 2015, **113**, 227.
53 H. Wang, J.-T. Ryu, Y. Kwon, *J. Appl. Polym. Sci.,* 2011, **119**, 377.
54 T.-Y. Wu, Y. Chen, *J. Polym. Sci., Part A: Polym. Chem.,* 2002, **40**, 3847.
55 A. D. Becke, *J. Chem. Phys.,* 1993, **98**, 1372.
56 M. M. Francl, W. J. Pietro, W. J. Hehre, J. S. Binkley, M. S. Gordon, D. J. DeFrees, J. A. Pople, *J. Chem. Phys.,* 1982, **77**, 3654.
57 Q. Tao, Y. Xia, X. Xu, S. Hedström, O. Bäcke, D. I. James, P. Persson, E. Olsson, O. Inganäs, L. Hou, W. Zhu, E. Wang, *Macromolecules,* 2015, **48**, 1009.
58 B. Pépin-Donat, C. Ottone, C. Morell, C. Lombard, A. Lefrançois, P. Reiss, M. Leclerc, S. Sadki, *J. Phys. Chem. C,* 2014, **118**, 20647.
59 P. M. Beaujuge, H. N. Tsao, M. R. Hansen, C. M. Amb, C. Risko, J. Subbiah, K. R. Choudhury, A. Mavrinskiy, W. Pisula, J.-L. Brédas, F. So, K. Müllen, J. R. Reynolds, *J. Am. Chem. Soc.,* 2012, **134**, 8944.
60 J. S. Wu, Y. J. Cheng, T. Y. Lin, C. Y. Chang, P. I. Shih, C. S. Hsu, *Adv. Funct. Mater.,* 2012, **22**, 1711.
61 B. Nketia-Yawson, H.-S. Lee, D. Seo, Y. Yoon, W.-T. Park, K. Kwak, H. J. Son, B. Kim, Y.-Y. Noh, *Adv. Mater.,* 2015, **27**, 3045.
62 J. Kim, M. H. Yun, G.-H. Kim, J. Lee, S. M. Lee, S.-J. Ko, Y. Kim, G. K. Dutta, M. Moon, S. Y. Park, D. S. Kim, J. Y. Kim, C. Yang, *ACS Appl. Mater. Interfaces,* 2014, **6**, 7523.
63 I. Osaka, R. Zhang, G. Sauvé, D.-M. Smilgies, T. Kowalewski, R. D. McCullough, *J. Am. Chem. Soc.,* 2009, **131**, 2521.
64 H. Sirringhaus, *Adv. Mater.,* 2009, **21**, 3859.
65 S. Cho, J. Yuen, J. Y. Kim, K. Lee, A. J. Heeger, *Appl. Phys. Lett.,* 2006, **89**, 153505.
66 N. B. Kolhe, A. Z. Ashar, K. S. Narayan, S. K. Asha, *Macromolecules,* 2014, **47**, 2296.
67 F. S. Kim, X. Guo, M. D. Watson, S. A. Jenekhe, *Adv. Mater.,* 2010, **22**, 478.
68 T. Yasuda, T. Imase, T. Yamamoto, *Macromolecules,* 2005, **38**, 7378.

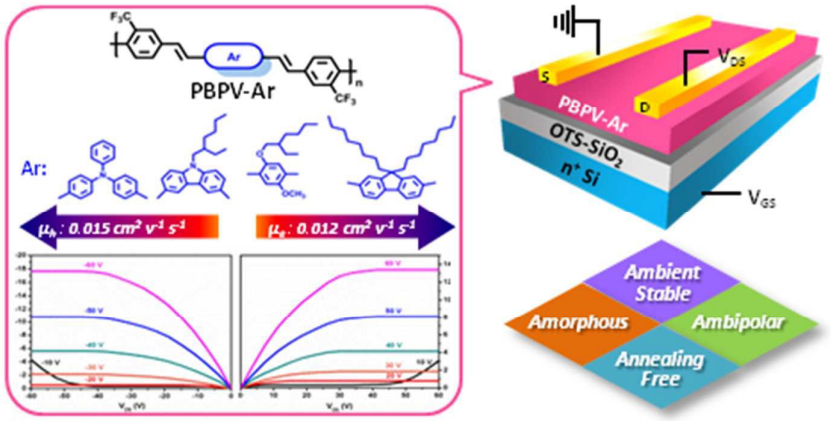

Ambipolar and annealing-free OFETs with high ambient-stability are achieved by introducing 2,2'-bis(trifluoromethyl)biphenyl as the acceptor.